AAPG BULLETIN

Effective flow properties of heterolithic, cross-bedded tidal sandstones: Part 2. Flow simulation

Benoit Y. G. Massart, Matthew D. Jackson, Gary J. Hampson, and Howard D. Johnson

AAPG Bulletin published online 12 February 2016
doi: 10.1306/02011614222

Cite as: Massart, B. Y. G., M. D. Jackson, G. J. Hampson, and H. D. Johnson, Effective flow properties of heterolithic, cross-bedded tidal sandstones: Part 2. Flow simulation, *(in press; preliminary version published online Ahead of Print* 12 February 2016*):* AAPG Bulletin, doi: 10.1306/02011614222.

Effective flow properties of heterolithic, cross-bedded tidal sandstones: Part 2. Flow simulation

Authors: **BENOÎT Y. G. MASSART[1,2]*, MATTHEW D. JACKSON[1], GARY J. HAMPSON[1], HOWARD D. JOHNSON[1]**

[1] Department of Earth Science and Engineering, Imperial College London, South Kensington Campus, London SW7 2AZ, UK.

[2] Current address: Statoil ASA, Sandsliveien 90, Bergen 5254, Norway.

*E-mail of corresponding author: bmass@statoil.com

Acknowledgements

Funding of the study, and approval for publication, by Shell Norway, Statoil, Total and Petoro, are gratefully acknowledged. The authors thank Schlumberger for providing the Petrel software used for visualization of the models, and Eclipse 100 software used for flow simulation. Similarly, the authors thank Roxar for providing the RMS software that was used for visualization. The authors acknowledge the contributions of Rodmar Ravnås (Norske Shell) and Marcus Sarginson (Murphy Sarawak Oil Company) for advice and guidance in the research project, as well as M.Sc. students Rui Hou and Oluwole Talabi (Imperial College London). We gratefully acknowledge C. Hern, M. Sweet, F. Whitehurst and two anonymous reviewers for their constructive reviews and editorial comments.

Abstract

Tidal heterolithic sandstone reservoirs are heterogeneous at the sub-meter scale, due to the ubiquitous presence of intercalated sandstone and mudstone laminae. Core-plug permeability measurements fail to sample a representative volume of this heterogeneity.

Here we investigate the impact of mudstone drape distribution on the effective permeability of heterolithic, cross-bedded tidal sandstones using three-dimensional (3D) surface-based "mini-models" that capture the geometry of cross-beds at an appropriate scale. The impact of seven geometric parameters has been determined: (1) mudstone fraction, (2) sandstone laminae thickness, (3) mudstone drape continuity, (4) toeset dip, (5) climb angle of foreset-toeset surfaces, (6) proportion of foresets to toesets, and (7) trough or tabular geometry of the cross-beds.

We begin by identifying a representative elementary volume (REV) of 1 m^3, confirming that the model volume of 9 m^3 yields representative permeability values. Effective permeability decreases as the mudstone fraction increases, and is highly anisotropic: vertical permeability falls to c. 0.5% of the sandstone permeability at a mudstone fraction of 25%, while the horizontal permeability falls to c. 5% and c. 50% of the sandstone value in the dip (across mudstone drapes) and strike (parallel to mudstone drapes) directions, respectively. There is considerable spread around these values, because each parameter investigated can significantly impact effective permeability, with the impact depending upon the flow direction and mudstone fraction. The results yield improved estimates of effective permeability in heterolithic, cross-bedded sandstones, which can be used to populate reservoir-scale model grid blocks using estimates of mudstone fraction and geometrical parameters obtained from core and outcrop-analog data.

Introduction

Tidal influence commonly results in the rhythmic deposition of sandstone and mudstone laminae in shallow-marine depositional environments (Nio and Yang, 1991). These mudstone

49 laminae (often termed “drapes”) affect the reservoir performance of tidal heterolithic
50 sandstone units, as they can act as baffles or barriers to flow during hydrocarbon
51 production, depending on their lateral and vertical extent (Weber, 1982; Kjønsvik *et al.*,
52 1994; Jackson and Muggeridge, 2000; White *et al.*, 2004; Martinius *et al.*, 2005;). Mudstone
53 drapes occur over a range of length-scales and with different geometric configurations,
54 reflecting the scale of bedforms and the strength and spatial variability of tidal currents
55 during deposition. Consequently, mudstone and sandstone laminae exhibit complex 3D
56 architecture with highly variable lateral and vertical connectivity that is challenging to
57 represent in geologic and flow-simulation models. Common practice is to obtain rock
58 properties for these heterogeneous sandstones from subsurface wireline-log data or
59 laboratory core measurements, and then to upscale these measurements to the grid-block
60 scale in geologic models using simple averaging methods (Corbett and Jensen, 1992). Yet
61 previous studies have demonstrated that averaging of core permeability measurements
62 does not yield representative values at the grid-block scale, because these data do not
63 sample a volume of rock that is representative of the heterogeneity (Jackson *et al.*, 2003).
64 Values appropriate for use at larger length-scales must be derived using a representative
65 elementary volume (REV) of the rock (sensu Bear, 1972): above this minimum volume,
66 measured or calculated properties are independent of the sample volume considered
67 (Figure 1). The REV for permeability must be sufficiently large to capture the key
68 heterogeneities dictating flow in all directions. In practice the REV may not be reached
69 before another scale of heterogeneity is encountered, making it difficult or impossible to
70 identify (Nordahl and Ringrose, 2008).

71 In previous studies, models of small (but larger than core) volumes (27 – 180 x 10^3 cm^3)
72 of wavy-bedded tidal sandstones have been generated using a geometric forward modelling

73 approach that mimics the movement of bedforms during deposition (Wen *et al.*, 1998, after
74 Rubin, 1987), in order to simulate flow and thus predict effective permeability in the near
75 wellbore region (Ringrose *et al.*, 2003, 2005; Nordahl *et al.*, 2005). The same models were
76 also used to determine an REV of 5 x 10^3 cm^3 for wavy-bedded tidal sandstones of varying
77 mudstone content (Nordahl and Ringrose, 2008). A surface-based modelling technique was
78 used by Jackson *et al.* (2005) to recreate realistic 3D models of flaser- and lenticular-bedded
79 tidal sandstones directly from outcrop rock samples. The two 7.5 x 10^4 cm^3 samples (0.5 x
80 0.5 x 0.3 m; i.e. above the REV of Nordahl and Ringrose, 2008) were serially-sectioned at a
81 spacing of 2 cm, and the surfaces bounding sandstone and mudstone lithologies traced in 2D
82 on each section, in order to reconstruct the lithologic-boundary surfaces in 3D (Jackson
83 *et al.*, 2005). Flow simulation of the resulting surface-based models identified the
84 connectivity of sandstone and mudstone laminae as the main parameter controlling
85 reservoir properties. Thus, accurate representation of sandstone- and mudstone-laminae
86 distribution and geometry is an essential requirement for models to predict effective
87 permeability.

88 In a companion paper (Massart *et al.*, 2016, this issue), we document a new surface-
89 based methodology for accurate geometric representation of lithologic heterogeneity in
90 heterolithic, cross-bedded tidal sandstones. The method requires the user to define input
91 values for a small number of parameters that describe the geometry and spatial distribution
92 of foreset-toeset surfaces and the distribution of mudstone drapes along these surfaces.
93 Values of the parameters may be derived for a given interval from a combination of wireline
94 and/or core and outcrop-analog data. In this paper, we apply the surface-based
95 methodology to construct a range of models of cross-bedded tidal sandstones, in order to
96 investigate the impact on effective permeability of mudstone drapes along foreset-toeset

surfaces within cross-beds. The study has four aims: (1) to identify a possible REV for heterolithic, cross-bedded tidal sandstones by investigating the impact of sample volume on permeability, (2) to quantify the impact on effective permeability of mudstone proportion, which is controlled by mudstone drape extent and continuity along foreset-toeset surfaces, (3) to determine whether effective permeability can be predicted to reasonable accuracy based only on knowledge of the sandstone fraction (the net-to-gross ratio), and (4) to assess the relative sensitivity of effective permeability to six geometric parameters that are uncertain in the subsurface but control the spatial arrangement of mudstone drapes in tidal cross-bedded heterolithic sandstones, and identify which of these, if any, are key to predicting effective permeability.

Methodology

Surface-based model construction

Models of cross-bedded heterolithic sandstones measuring 3 x 3 x 1 m (9 m^3) were generated for this study using the surface-based methodology presented in the companion paper (Massart *et al.*, 2016), so only a brief outline of the methodology is provided here. The methodology follows four key steps:

Model cross-bed sets and cross-bed surfaces within sets. The volume of interest is subdivided into ellipsoidal cross-bed sets, each defined by one base and one top surface. The spatial distribution of the cross-bed sets can be modelled stochastically (i.e. cross-bed sets are placed randomly into the model volume, and the dimensions and orientations of each are drawn from an input distribution) or deterministically (location, orientation and

120 dimensions for each are user-specified). The base of each cross-bed set is erosional, so cross-
121 bed sets erode into each other following the rules of stratigraphic order. Numerous cross-
122 bed surfaces (termed here "foreset-toeset surfaces") with a common geometry are then
123 modelled within each cross-bed set, until a specific density (number per unit volume) is
124 reached. The geometric input parameters required to model the foreset-toeset surfaces are:
125 (1) the foreset thickness F_T and (2) the toeset thickness T_T between two successive foreset-
126 toeset surfaces; (3) the toeset dip angle α; (4) the dune climb angle δ; and (5) the foreset
127 curvature, defined by the characteristic parameter A of a parabolic curve with equation $z(x) = Ax^2$
128 (see Figure 5 in Massart *et al.*, 2016).

129 Grid the model volume for flow simulation. The surface-based models are gridded using
130 corner-point grids in which the grid layers are constrained by the modelled foreset-toeset
131 surfaces, which ensures their complex geometries are preserved. In the models presented
132 here, the grid cells measure 5 x 5 x 2 cm, except for the cells immediately above a foreset-
133 toeset surface, which have a thickness of 0.35 cm to model the mudstone drapes (described
134 below). The volume between two successive foreset-toeset surfaces is divided into layers of
135 cells that are aligned parallel to the underlying foreset-toeset surface. The model contains
136 numerous zero-thickness cells, which occur where foreset-toeset surfaces downlap onto, or
137 are truncated by, cross-bed set bounding surfaces. These zero-thickness cells are inactive
138 and are bridged using non-neighbor connections (cf. White and Barton, 1999; Jackson *et al.*,
139 2005, 2009; Sech *et al.*, 2009).

140 Model sandstone and mudstone lithologies. The lithology is assumed to be sandstone
141 except where mudstone layers are present. More or less continuous mudstone layers are
142 modelled stochastically along foreset-toeset surfaces to represent mudstone drapes

deposited during slack-water periods on pre-existing bedforms. The thin (0.35 cm) grid layer directly above each foreset-toeset surface is used to incorporate mudstone drapes, which are documented to have a comparable thickness (Terwindt, 1971; Nio and Yang, 1991; Martinius and Van den Berg, 2011). Because mudstones are modelled as barriers to flow (see below), their thickness has no impact on their flow properties; however, it does affect the total volume of the model that is occupied by mudstone for a given coverage of foreset-toeset surfaces. Mudstone drapes are modelled as elliptical patches that cover the foreset-toeset surfaces until a user-specified proportion of their area is reached, following the methodology of Jackson and Muggeridge (2000). A mudstone frequency function, extracted from outcrop data, is used to constrain the probability that a given location on each surface is occupied by a mudstone drape (see Figure 12 in Massart *et al.*, 2016).

Model petrophysical properties. The sandstone and mudstone lithologies are each modelled with uniform, isotropic permeability and the value is zero in mudstone, consistent with minipermeameter measurements that show mudstone permeability is often below instrument resolution (< 1 nd) and at least five orders of magnitude lower than sandstone permeability in a given sample (e.g. Ringrose *et al.*, 2005). This approach yields models in which toesets contain laterally extensive sandstone laminae separated by mudstone drapes, analogous to wavy-bedded toesets. However, previous studies have shown that the lateral sandstone connectivity breaks down when the sandstone fraction falls below c. 0.29 (corresponding to the percolation threshold; King, 1990), in which case sandstones form isolated lenses comprising lenticular-bedding (Jackson *et al.*, 2005). Consequently, in toeset regions, the sandstone permeability is set to zero if the volumetric sandstone fraction is less than 0.29, to mimic the lack of lateral connectivity in lenticular-bedded toesets. Note that,

for the single-phase permeability calculations reported here, the sandstone porosity plays no role.

Identification of the REV for heterolithic, cross-bedded tidal sandstones

The impact of sample volume on effective permeability was determined in order to identify a potential REV. The model chosen for this analysis is referred as the "intermediate model". Geometric input parameters for this model were obtained from a specific locality (termed "Gecko Nose") within the outcrop analog (the Eocene Dir Abu Lifa Member in the Western Desert, Egypt; Legler *et al.*, 2013) from which the modelling methodology was derived. The input parameters correspond to the average of the ranges measured at the outcrop location (Table 1). The model represents trough cross-bedding with a mudstone drape coverage of 25% along foreset surfaces and 57% along toesets. The corresponding sandstone proportion (the net to gross ratio) is 0.89. The largest modelled volume is 9 m^3 (3 x 3 x 1 m), which contains 6 cross-bed sets (with partially preserved, elliptical geometry in dip-oriented and strike-oriented cross-sections), and approximately 600 foreset-toeset surfaces. The foreset-toeset surfaces have realistic geometries and realistic terminations at the boundaries of the cross-bed sets. The corresponding corner-point grid has approximately 6 million cells, of which 700,000 are active for flow simulation (Figure 2). The resolution of the grid has been chosen in order to reproduce accurately the complex geometry of the foreset-toeset surfaces, especially at their terminations, and to keep the number of cells sufficiently small for flow simulation.

The model was subdivided into smaller samples, each sharing a common center point, and the effective permeability was determined following the methodology presented below.

189 The smallest sample volume investigated was 0.009 m^3 which corresponds to a typical core
190 plug. The corner-point grid architecture remained the same in each model, so the number of
191 cells varied with sample volume, with the smallest sample containing 1000 active cells.

192

193 ***Impact of mudstone drape coverage on effective permeability***

194 To determine whether effective permeability can be predicted from measurements of
195 sandstone fraction (i.e. net-to-gross ratio), the intermediate model described above was
196 used to study the impact of mudstone drape coverage along foreset-toeset surfaces on
197 effective permeability. The mudstone drape coverage was varied from 100% to 0%; the
198 corresponding fraction of sandstone in the model varied from 0.74 (when all foreset-toeset
199 surfaces are entirely covered by mudstone drapes) to 1.00 (no mudstone drape). Effective
200 permeability was calculated using the method described below in three orthogonal
201 directions: two perpendicular horizontal directions, parallel (dip direction) and perpendicular
202 (strike direction) to the orientation of the foreset-toeset surfaces, and the vertical direction.
203 This methodology is similar to those used in previous studies of the impact of mudstone
204 fraction on effective permeability for wavy-bedded heterolithic tidal sandstones (Jackson
205 *et al.*, 2003; Ringrose *et al.*, 2003, 2005; Nordahl *et al.*, 2005). By varying the mudstone
206 drape coverage, we directly changed the mudstone content of the model without changing
207 the geometry of the stratigraphic surfaces. In this way, it was possible to determine whether
208 cross-bedded heterolithic sandstones behave in accordance with a percolation threshold
209 (King, 1990), as noted in models of wavy-bedded heterolithic sandstones (Jackson *et al.*,
210 2005).

211

Impact of mudstone-drape coverage on effective permeability in trough and tabular cross-bedded end-member models

In addition to the intermediate model described above, two geologically plausible end-member models were created to determine the possible range of effective permeability for tidal cross-bedded sandstones, depending on the style of cross-bedding, the geometry and distribution of foreset-toeset surfaces in cross-bed sets, and the connectivity of sandstone laminae in the toeset areas. One model represents trough cross-bedded sandstone with prominent toeset areas (foreset to toeset volume ratio $R_{F/T}$ = 2 : 3) (Table 1; Figure 3); as for the intermediate model, the input data were obtained from the Gecko Nose outcrop location described in the companion paper (Massart *et al.*, 2016). The other end-member model represents tabular cross-bedded sandstone with almost non-existent toeset areas (foreset to toeset volume ratio $R_{F/T}$ = 24 : 1) (Table 1; Figure 4); input data for this model were obtained from the Butterfly Canyon location described in the companion paper (Massart *et al.*, 2016). This model is also presented in the companion paper (see Figure 14 in Massart *et al.*, 2016).

The settings of the six input parameters for these two end-member models are summarized in Table 1; they were taken from the outcrop data reported in the companion paper (Massart *et al.*, 2016). The foreset thickness F_T distribution was chosen to be log-normal with a standard deviation $\sigma(F_T)$ of 3.9 cm in both trough and tabular cross-bedded models, but with a different mean value, specific to the outcrop location. The foreset thickness directly impacts the number of foreset-toeset surfaces contained in a cross-bed set. Mud-patch ellipse dimensions were drawn from uniform distributions that yielded mudstone drapes in the trough cross-bedded end-member model that were elongated and continuous, and mudstone drapes in the tabular cross-bedded model that were

236 discontinuous and mostly preserved in the toesets and distal foresets. Multiple mudstone
237 drape coverage scenarios were created for both end-member models. Effective permeability
238 was then determined as described above for each model with varying mudstone drape
239 coverage.

240

241 ***Sensitivity analysis of geometric parameters***

242 The final step of the work undertaken here was to investigate the sensitivity of effective
243 permeability to uncertain parameters controlling the geometry of the foreset-toeset
244 surfaces with a combination of settings, which represent a spread of cross-bed architectures
245 around the intermediate case and within the range spanned by the end-member cases. The
246 following six parameters were varied in the sensitivity analysis, between the end-member
247 settings reported in Table 1: (1) the style of cross-bedding (trough or tabular cross-bedding);
248 (2) the volume ratio between sandy foresets and muddy toesets $R_{F/T}$; (3) foreset thickness
249 F_T; (4) toeset dip angle α; (5) angle of dune climb δ; and (6) the length of elliptical mudstone
250 patches placed along foreset-toeset surfaces MP_L. An experimental design approach was
251 used, which allows the relative effects of different variables to be quantified whilst
252 minimizing the number of simulation experiments (Box and Draper, 1987; White *et al.*,
253 2001). A two-level fractional-factorial experimental design was selected, which yielded nine
254 ($2^{(6-3)}$+1) different models, and allowed the main effects of each individual parameter to be
255 determined, but not the interaction effects (i.e. the combined effect of varying two or more
256 parameters simultaneously). For each of the nine models created, three mudstone drape
257 coverage scenarios were tested, and the effective permeability was determined in the
258 horizontal dip and strike directions.

Calculation of effective permeability

Effective permeability was calculated in all models and in all three flow directions (dip, strike and vertical) by simulating single phase flow using a conventional industry simulator (Schlumberger, 2013) and calculating the effective permeability k_e using Darcy's Law expressed as (e.g. Warren and Price, 1961):

$$k_e = \frac{Q\mu L}{A\Delta P} \quad (1)$$

where Q is the volumetric flow rate (m^3/s), μ is the viscosity (chosen arbitrarily to be 1 Pa.s), L is the model length in the direction of flow (m), A is the cross-sectional area of the model perpendicular to the direction of flow (m^2), and ΔP is the fluid potential drop along the model in the direction of flow (Pa). The fluid potential corresponds to the fluid pressure minus the hydrostatic pressure.

To calculate permeability in a given direction, fluid was injected into one face of the model and produced from the opposing face; the other four model faces were sealed. Horizontal flow parallel to the main orientation of the cross-bedding surfaces is termed dip-oriented and the permeability is denoted k_d; the perpendicular, horizontal direction is termed strike-oriented, and the permeability is denoted k_s. The horizontal permeability k_h has been defined as the arithmetic mean between k_d and k_s ($k_h = (k_d + k_s)/2$) as it is usually the favorite averaging method for estimating horizontal permeability (Jackson *et al.*, 2003). Vertical effective permeability is denoted k_v. Injection and production faces contained a single layer of high permeability buffer cells (arbitrarily chosen to be 54 x 10^3 d) to ensure that flow was uniformly distributed and the fluid potential was uniform. A single injection-production well pair was defined at the inlet and outlet faces respectively; the injection rate

was limited by a maximum pressure, which was higher than the (atmospheric) outlet pressure, while the production rate was controlled by a fixed target. Each simulation was run until a steady-state was reached, at which injection and production rates were the same (within a tolerance of 1%) and the average fluid potential was constant (within a tolerance of 1% between timesteps). The rock and fluid had a small but non-zero compressibility, which allowed the simulator to converge to a stable solution more rapidly at each time-step whilst reaching steady-state within a short time (typically < 10^{-6} pore-volumes of fluid injected). At steady state, the flow rate Q and fluid potential drop ΔP were determined and the effective permeability calculated using equation (1). Values of effective permeability k_e in a given direction are reported as a normalized value expressed as a fraction of the isotropic sandstone permeability k_{sand}:

$$k_e^n = \frac{k_e}{k_{sand}} \quad (2)$$

The results reported in this way are independent of the value of sandstone permeability used in the models; moreover, the normalized effective permeability can be rescaled to any value of sandstone permeability obtained from core-plug or mini-permeameter measurements.

The corner-point grids used to capture the complex architecture of the cross-beds contain relatively steeply inclined cells. Thus, while the grids accurately reproduce stratigraphy and heterogeneity in the models, they also cause numerical artefacts to be introduced by the flow simulator because the cells deviate from k-orthogonality (e.g. Jackson *et al.*, 2015). The magnitude of these numerical grid-geometry errors was calculated using a reference model in which mudstone drapes are entirely absent (i.e. sandstone fraction equal to 1.00) but the corner-point grid represents the architecture of the cross-beds. The

effective permeability of the reference model should be that of sandstone in the three directions of simulated flow. Differences between this and the numerically calculated value yield estimated errors in k_d of 25%, k_s of 1%, k_v of 16%, and k_v/k_h of 26%. Numerical errors in cases where the mudstone fraction is greater than zero are assumed to be the same as these determined for the reference model as the errors are introduced solely by the grid geometry. The error in the dip and vertical directions is relatively large, and reflects the high deviation from *k*-orthogonality in these directions. The error is not reduced by grid refinement, because this does not reduce the deviation from *k*-orthogonality. Various approaches for reducing the grid geometry error were tested, including the use of a multi-point flux approximation (MPFA) option in the reservoir simulator, but the pressure solution using this option failed to converge.

Results

Visualization and qualitative analysis

The intermediate model and the two end-member models can be visualized using industry-standard geomodelling software for qualitative analysis of the heterogeneity surface geometry and mudstone distribution. The intermediate model and the tabular cross-bedded end-member model were briefly presented in the companion paper (see Figures 13 and 14 in Massart *et al.*, 2016); the trough cross-bedded end-member model has not been reported previously. Here we discuss and compare their features.

The intermediate (Figure 2) and the trough cross-bedded end-member (Figure 3) models were generated from the same outcrop location (Gecko Nose, see Figure 8 in Massart *et al.*, 2016). As the foreset thickness F_T is specific to the outcrop location, its mean value is the same for both models (F_T = 5.9 ± 3.9 cm) with a progressive transition (from thin to thick sandstone laminae, and then back to thin laminae) corresponding to a neap-spring tidal cycle. The trough cross-bedded end-member model displays a higher density network of mudstone drapes than the intermediate model (compare Figures 2 and 3) even though the foreset spacing is the same in both models; the difference arises in the volume fraction occupied by muddy toeset parts, with the toeset volume proportion of the trough cross-bedded end-member model (60%) being 4.5 times higher than that of the intermediate model counterpart (13%) (Table 1). The trough cross-bedded end-member model is directly recreated from one outcrop example of the Gecko Nose outcrop location featuring this high proportion of muddy toeset parts (Figure 3 A), whereas the foreset to toeset volume ratio for the intermediate model is an average of all measured trough cross-bed sets at the Gecko Nose outcrop. As mudstone drapes are more continuous in the toesets, 3D connectivity

between sandstone laminae is more limited in the trough cross-bedded end-member model than in the intermediate model.

The tabular cross-bedded end-member model was generated from the Butterfly Canyon location (see Figure 6 in Massart *et al.*, 2016). In this model, sandy foreset parts are predominant over the muddy toeset parts, with a toeset volume proportion of 4% reproduced directly from one example at the outcrop location (Figure 4). The mean foreset thickness F_T is higher for this model with F_T = 10.0 ± 3.9 cm. Consequently, mudstone content in the model only reaches a volume fraction of 0.13 when foreset-toeset surfaces are entirely covered by mudstone drapes (i.e. at 100% mudstone drape coverage).

The appearance of the muddy toesets is different between the Gecko Nose and the Butterfly Canyon outcrop locations, and is reproduced accordingly in the models reported here. Toesets at Butterfly Canyon are limited to thin but laterally continuous mudstone drapes that occur between stacked cross-bed sets (Figure 4 A) and are reproduced as such in the tabular cross-bedded end-member model (Figure 4 D). At Gecko Nose, toesets are well expressed, comprising alternate, parallel sandstone and mudstone laminae (i.e. mudstone drapes along toeset surfaces) yielding wavy-bedding structures (Reineck and Singh, 1980; Ringrose *et al.*, 2005) (Figure 3 A), and reproduced in the trough cross-bedded end-member model (Figure 3 D) as well as the intermediate model. This difference in toeset content is reflected in the values of toeset dip angle α and dune climb angle δ (Table 1). The smaller these two angles are, the thinner the toeset thickness T_T (equation (6) in Massart *et al.*, 2016). As both values of α and δ are small, the toeset thickness T_T in the tabular cross-bedded end-member model is very small. In this model, mudstone drapes stack vertically with few sandstone laminae preserved in-between; moreover, as the dune climb angle δ is

363 equal to 0, toeset surfaces merge with the erosional base of the cross-bed sets, forming the
364 observed continuous mudstone drapes that serve to isolate vertically stacked cross-bed sets.

365 ***Impact of sample volume on effective permeability***

366 We begin by presenting typical results for one flow simulation experiment, yielding a
367 single value of effective permeability (Figure 5). The example is for the intermediate model
368 with 25% mudstone drape coverage, the full sample volume of 9 m^3, and flow in the (down)
369 dip direction (i.e. across mudstone drapes). Flow rate and average fluid potential are
370 reported as a function of pore-volumes of fluid injected (PVI). It is clear that the injection
371 and production flow rates rapidly reach steady state, as does the average fluid pressure. At
372 this time, the simulated flow rate and potential drop can be used in equation (1), along with
373 the model dimensions and fluid viscosity, to calculate the effective permeability.

374 Numerous numerical experiments of this type, with flow in different directions and using
375 different sample volumes, yielded the values of normalized effective permeability for the
376 intermediate model shown in Figure 6; also shown is the sandstone fraction in the
377 corresponding model. The variability in permeability is a function of sample volume, as is the
378 fraction of sandstone. This latter variation occurs because different volumes of mudstone
379 are included in models as the sample volume changes. Horizontal permeability in both dip
380 and strike orientations varies with the volume of the sample, for sample volumes below
381 1 m^3. A sample volume of c. 1 m^3 thus corresponds here to the REV. The slight increase in
382 effective permeability observed for increasing sample volumes above 1 m^3 (Figure 6) is
383 attributed to the increase in sandstone proportion as more sandy foresets are sampled
384 towards the edges of the model, because the permeability variations observed for the

385 sample models of volume > 1 m^3 follow the same trend as the sandstone proportion
386 variations.

387

388 ***Impact of sandstone fraction on effective permeability***

389 The effective permeability of the intermediate model (Figure 2) was calculated for 33
390 scenarios of mudstone drape coverage along foreset-toeset surfaces, ranging from 0% to
391 100%, corresponding to sandstone proportions ranging from 1.00 to 0.74 respectively.
392 Normalized effective permeability is dependent on the proportion of sandstone, and on the
393 direction of flow relative to the foreset-toeset surfaces (Figure 7). Effective permeability
394 decreases as the sandstone fraction decreases and is highly anisotropic: the vertical
395 permeability falls to c. 0.5% of the value for sandstone, while the horizontal permeability
396 falls to c. 5% and c. 50% of the sandstone value in the dip and strike directions, respectively.

397 For high proportions of sandstone (> 94%), mudstone drapes occur only along toesets,
398 and k_d and k_s are similar. For low proportions of sandstone (< 94%), in which both foresets
399 and toesets are lined by mudstone drapes, k_d and k_s differ such that horizontal effective
400 permeability is anisotropic. The horizontal effective permeability along depositional strike,
401 k_s, is higher than along depositional dip, k_d, because sandstone laminae are more laterally
402 continuous along strike. Dip-oriented, horizontal flow within each cross-bed set must cross
403 multiple, mudstone-draped foreset-toeset surfaces that increase tortuosity and may create
404 dead-ends, especially for high mudstone contents (e.g. Figures 3 C, 4 C). Dead-ends for flow
405 in the strike direction occur where sandstone laminae of foreset areas are juxtaposed
406 against mudstone laminae of toeset areas across an erosional cross-bed set boundary.

407 The vertical effective permeability k_v is generally much lower than both k_d and k_s. This
408 effect is attributed to the presence of mudstone drapes along toesets, which are nearly
409 horizontal and closely spaced such that they act as barriers or baffles to vertical flow, even in
410 models with low mudstone content. As a result, the decrease in k_v with increasing mudstone
411 content is similar to that documented for wavy-bedded sandstones, with a high decrease in
412 the effective vertical permeability accompanying a small increase in mudstone fraction
413 (Nordahl *et al.*, 2005; Ringrose *et al.*, 2005). Variations in the ratio between vertical and
414 horizontal effective permeability k_v/k_h , as a function of sandstone content, are mainly
415 controlled by the variations in k_v.

416

417 ***Impact of varying mudstone-drape coverage on effective permeability in end-member***
418 ***models of tabular and trough cross-bedding***

419 The normalized horizontal effective permeabilities for the trough cross-bedded end-
420 member model (Figure 3) and the tabular cross-bedded end-member model (Figure 4) are
421 shown in Figure 8 for two different toeset bedding styles: in wavy-bedded toesets, the
422 sandstone and mudstone layers are laterally continuous; in lenticular-bedded toesets, the
423 sandstones form isolated lenses encased in mudstone. Also shown for comparison are the
424 results for the intermediate model with wavy-bedded toesets, which correspond to the
425 results of Figure 7.

426 The anisotropy in horizontal permeability observed in the intermediate model is
427 amplified by the geometry of the cross-beds in the end-member models, especially for the
428 dip direction k_d (Figure 8 A). The dip-oriented effective permeability decreases linearly and
429 rapidly with increasing mudstone content for the tabular cross-bedded model regardless of

the toeset bedding style, but decreases less rapidly for the trough cross-bedded model with wavy-bedded toesets (Figure 8 A) and is very low in this model with lenticular-bedded toesets (Figure 8 C). In contrast, effective permeability in the strike direction k_s is similar for all three models if they have wavy-bedded toesets (Figure 8 B), but differs significantly if they have lenticular-bedded toesets (Figure 8 D). The large range of effective permeability values between the two (realistic) end-member models confirms the strong influence of toeset lamination style on the horizontal anisotropy in effective permeability.

Values of effective permeability are modified profoundly by the lateral continuity of sandstone and mudstone laminae in the toesets (wavy- versus lenticular-bedding; compare Figure 8 A and B with Figure 8 C and D), with the exception of the tabular cross-bedded end-member model in which toesets are volumetrically subordinate, yet k_v is the smallest due to the stacking of the mudstone drapes into relatively thick mudstone layers at the bottom of cross-bed sets. The same value of sandstone fraction gives very different values of effective permeability, depending on the geometry of cross-bedding, the bedding style of the toeset parts, the foreset thickness (which controls the number of mudstone drapes) and the direction of flow. For example, a sandstone fraction of 90% yields dip-oriented effective permeabilities k_d that are twice the value for the trough cross-bedded model (k_d = 0.72) than for the tabular cross-bedded model (k_d = 0.36) (Figure 8 A). For strike-oriented flow, k_s is the same as k_d for the trough cross-bedded model (k_s = 0.72) but higher for the tabular cross-bedded model (k_s = 0.87) (Figure 8 B). These results are extracted from models with wavy-bedded toesets; the results are different for lenticular-bedded toesets (Figure 8 C and D).

The spread of effective permeability values for any chosen model, independent of mudstone drape coverage, is controlled by the toeset regions of the model and their related

453 parameters: (1) the abundance of toeset region in the model, which is controlled essentially
454 by the foreset to toeset ratio (Table 1); (2) the lateral and vertical connectivity of toeset
455 regions in different cross-bed sets, which is controlled by various parameters (3D
456 distribution of cross-bed sets, cross-bed set density, and dune climb angle δ); and (3) the
457 wavy- or lenticular-bedded nature of the toesets, which is controlled by the mudstone drape
458 coverage and toeset dip angle α.

459

460 ***Influence of toeset bedding style on flow and effective permeability***

461 *End-Member Models with Wavy-Bedded Toesets*

462 The variation of the fluid potential at steady-state for models with wavy-bedded toesets
463 is illustrated in Figure 9 A, C and E. The fluid potential is influenced by the cross-bedding
464 surfaces, with high potentials located preferentially at the bottom of the models, adjacent to
465 the injection face; low potentials are located preferentially at the top of the models,
466 adjacent to the production face. This aspect of the fluid potential is related to the concave
467 geometry of the cross-bedding surfaces and the mudstone distribution along each surface:
468 the lower parts of the surfaces tend to be lined with mudstone drapes, leading to locally
469 higher potentials; in comparison, the comparatively mudstone-free, upper parts of the
470 surfaces constitute pathways for flow, leading to locally lower potentials. In areas where the
471 flow is driven down the cross-bedding surfaces, wavy-bedded layers in the toeset regions
472 allow the flow to reach underlying cross-bed sets. As a result, all the sandstone laminae of
473 the model are connected. Flow pathways may be highly distorted by an increase of
474 mudstone drape coverage, but there are no dead-ends to flow.

475

End-Member Models with Lenticular-Bedded Toesets

The variation of the fluid potential at the steady state for models with lenticular-bedded toesets is illustrated in Figure 9 B, D and F. In all models, the lenticular-bedded toesets stack vertically, isolating adjacent cross-bed sets and creating dead-ends to horizontal flow. Noticeably, in the trough cross-bedded model (Figure 9 B), only the lowermost cross-bed set is connected to both the injection and production faces; this cross-bed set constitutes the dominant flow path. The tortuosity of the flow is primarily controlled by the abundance of toesets compared to foresets; the foreset mudstone drape coverage has an impact only in cases where toesets are comparatively scarce (for example, in the tabular cross-bedded models, Figure 9 E and F).

Sensitivity analysis of effective permeability to various cross-bedding geometric parameters

The results of the experimental design to investigate the relative impact of six geometric parameters on effective permeability are presented in Figure 10. With increased mudstone drape coverage along foreset-toeset surfaces, it can be observed that: (1) the rank order of impact of the six parameters varies in both k_d and k_s; (2) the rank order differs between k_d and k_s; (3) the majority of the parameters induce a change of more than 10% on effective permeability; and (4) the only parameter with a consistently low impact on effective permeability is foreset thickness F_T. Each of the other parameters affects the effective permeability significantly in either the dip or strike direction. A decrease in F_T causes an increase in the number of foreset-toeset surfaces and the number of mudstone drapes that can potentially influence flow behavior. The consistently low ranking of F_T therefore suggests

499 that foreset regions have only limited impact on effective permeability compared to toeset
500 regions. This inference is supported by the greater impact on effective permeability of the
501 other five parameters, which each have a direct influence on the proportion, distribution
502 and connectivity of toeset regions. Overall these results show that effective permeability is
503 not controlled by just one or two key geometric parameters.

504

505 ## Discussion

506 The results presented here demonstrate that values of effective permeability for
507 heterolithic cross-bedded sandstones are highly sensitive to only small variations in
508 geometry and mudstone content. Calculated values of effective permeability were highly
509 variable in realistic models of the same interval, constructed using data extracted from
510 different outcrop locations. Predictive relationships for effective permeability as a function
511 of mudstone content were determined in earlier studies from mini-models of heterolithic,
512 wavy-bedded tidal sandstones, comparable in length-scale to the models presented here
513 (Ringrose *et al.*, 2005; Jackson *et al.*, 2005). However, such a relationship cannot be
514 identified for cross-bedded tidal sandstones, because mudstone content is not an indicator
515 of the cross-bed geometry, or the connectivity of sandstone or mudstone laminae. There is
516 no simple relationship that can be used to predict effective permeability in all heterolithic,
517 cross-bedded tidal sandstones based only on measurements of mudstone content or a small
518 number of geometric parameters.

519 The recommended workflow to calculate effective permeability in heterolithic, cross-
520 bedded tidal sandstones is therefore to create a number of mini-models, similar to those
521 presented in this study, that capture the range of cross-bedding styles, geometries and

522 mudstone content observed in reservoir-specific subsurface and outcrop analog data, and
523 calculate effective single phase (and multiphase, where necessary) reservoir properties from
524 these models following the "geopseudo" approach suggested in previous studies for
525 heterolithic sandstone reservoirs of other depositional environments (e.g. Ringrose *et al.*,
526 1993; Pickup *et al.*, 1994, 2000; Ciammetti *et al.*, 1995; Pickup and Carruthers, 1996; Pickup
527 and Sorbie, 1996). The models should capture rock volumes at, or greater than, the REV for
528 heterolithic cross-bedded tidal sandstones, which we find here to be of order 1000 x 10^3 cm^3
529 (1 m^3); for comparison, Nordahl and Ringrose (2008) identified a REV of order 5 x 10^3 cm^3 for
530 wavy-bedded tidal sandstones of varying mudstone content. The significantly larger REV that
531 we identify here reflects the lateral extent of mudstone drapes along foreset-toeset surfaces
532 and, in particular, the distribution and connectivity of muddy toesets that may themselves
533 comprise wavy- or lenticular-bedded intervals.

534 It should be noted that the size of the models tested in this study was limited to 9 m^3. As
535 a result, the existence of an REV at a larger length-scale, corresponding to stacked cross-bed
536 sets in an architectural element such as a barform, could not be verified. Moreover, the
537 impact of cross-bed set terminations, especially in the strike orientation, could not be
538 determined. The results of the sensitivity analysis revealed that the parameters controlling
539 the distribution and connectivity of mudstone in the toesets had a greater impact on
540 effective permeability than the parameters controlling the distribution of mudstone on the
541 foresets. Future studies could address the scale problem outlined above by creating generic
542 models of composite barforms, dividing the volume of interest into foreset-dominated and
543 toeset-dominated parts. Effective permeability values derived here for cross-bedded tidal
544 sandstones, and from previous studies for wavy-bedded tidal sandstones, could be assigned
545 respectively to the foreset-dominated and toeset-dominated parts of such barform models.

546 To constrain the effective permeability of tidal heterolithic cross-bedded sandstone
547 facies, the construction of mini-models can be facilitated using dedicated software focused
548 on process-based modelling of sedimentary architecture (noting the limitations outlined in
549 the introduction of this paper: it is difficult to ensure that process-based models honor
550 geometric data obtained from the subsurface or outcrop analogs), or the software
551 developed for this study. Some of the geometric parameters required to construct such
552 models can be extracted from subsurface data; others must be estimated or obtained from
553 outcrop analogs (e.g. Massart *et al.*, 2016). A broad range of geometric parameters is
554 expected, as heterolithic intervals vary laterally at the meter scale in tidally influenced
555 depositional environments. The impact of this variability on effective permeability is
556 illustrated by the differences observed in the two end-member models constructed in this
557 study using data from the same reservoir-analog formation.

558 In many circumstances, the creation of such mini-models will not be possible, and the
559 results of our study provide some semi-qualitative guidance to constrain effective
560 permeability in cross-bedded tidal sandstones when only core-plug measurements of
561 permeability are available. Critically, it is likely that the effective horizontal permeability will
562 be significantly lower than predicted from core-plug measurements (see also Jackson *et al.*,
563 2003, 2005), because plug-scale measurements over-estimate the lateral continuity of
564 sandstone laminae, and fail to account for the presence of muddy toesets that reduce lateral
565 connectivity. Even where the mudstone content is relatively low, the effective horizontal
566 permeability may be significantly reduced; for example, in the models investigated here, a
567 mudstone content of just 20% can reduce the effective horizontal permeability to 15 – 60%
568 of the sandstone value (Figures 7, 8); if the measured sandstone permeability was of order
569 100 md, the effective permeability would be of order 15 – 60 md. The decrease in vertical

permeability is typically even more severe: the same mudstone content of 20% can reduce the vertical permeability to just 2% of the sandstone value. Thus there is likely to be significant scope to reduce plug-derived values of permeability in a history match, or when comparing against permeability values interpreted from pressure transient data, even in relatively high net-to-gross intervals of cross-bedded tidal sandstones.

Conclusions

A suite of surface-based models of heterolithic, cross-bedded tidal sandstones has been investigated via flow simulation in order to calculate their effective permeability. Key findings are summarized below.

(1) Values of effective permeability are dependent on the volume sampled, but variation is minimized for sample volumes of greater than c. 1 m^3, which thus corresponds to a representative elementary volume for the cross-bedded, heterolithic tidal sandstone facies investigated here. No REV for larger geologic elements comprising such facies (e.g. barforms) could be identified over the maximum 9 m^3 volume of the models used.

(2) Variation in the coverage of foreset-toeset surfaces by mudstone drapes has an impact on effective permeability, and introduces pronounced anisotropy not only between horizontal and vertical permeability, but also between dip-oriented and strike-oriented horizontal permeability. Permeability anisotropy arises from the preferential occurrence of mudstone drapes along toesets, which are closely spaced near the base of cross-bed sets to form barriers to vertical flow even for small mudstone contents, and which bound sandstone laminae of greater continuity along depositional strike compared to down depositional dip.

(3) Variation in the continuity of sandstone laminae in the toeset regions of cross-bed sets is a critical control on effective permeability. The occurrence of discontinuous sandstone laminae in lenticular-bedded toesets results in flow occurring only through sandy foreset regions of cross-bed sets. The occurrence of continuous sandstone laminae in wavy-bedded toesets enables horizontal flow also through muddy toeset regions; furthermore, these laterally continuous sandstone laminae can be juxtaposed across erosional cross-bed set boundaries to enable flow between cross-bed sets.

(4) No single parameter describing cross-bedding geometry exerts a dominant control on effective permeability. Instead, five parameters that control the distribution, extent and geometric configuration of toesets exert significant influence on effective permeability for different sandstone proportions and flow directions: (1) trough or tabular cross-bedding style; (2) the volumetric ratio between foreset and toeset regions; (3) toeset dip angle; (4) angle of dune climb; and (5) the dimensions of mudstone drapes present along foreset-toeset surfaces. Parameters that control the distribution, extent and geometric configuration of foresets are less significant. The sensitivity of effective permeability to multiple geometric parameters indicates that it is best calculated using a range of models that capture the uncertainty in cross-bedding geometry. Input parameters for these models can be extracted from core and outcrop-analog data and the models can be constructed using the methodology and/or code described in the companion paper.

References cited

Bear, J., 1972, Dynamics of fluids in porous media, American Elsevier (New York).

Box, G. E. P., and N. R. Draper, 1987, Empirical model building and response surfaces, Wiley (New York).

Ciammetti, G., P. S. Ringrose, T. R. Good, J. M. L. Lewis, and K. S. Sorbie, 1995, Waterflood recovery and fluid flow upscaling in a shallow marine and fluvial sandstone sequence, SPE Annual Technical Conference, Dallas, USA, 22-25 October, Society of Petroleum Engineers paper 30783.

Corbett, P. W. M., and J. L. Jensen, 1992, Variation of reservoir statistics according to sample spacing and measurement type for some intervals in the lower Brent Group: The Log Analyst: v. 33, p. 22-41.

Jackson, M. D., and A. H. Muggeridge, 2000, The effect of discontinuous shales on reservoir performance during immiscible flow, Society of Petroleum Engineers Journal, v. 5, p. 446–454.

Jackson, M. D., A. H. Muggeridge, S. Yoshida, and H. D. Johnson, 2003, Upscaling permeability measurements within complex heterolithic tidal sandstones, Mathematical Geology, v. 35, p. 499-520.

Jackson, M. D., S. Yoshida, A. H. Muggeridge, and H. D. Johnson, 2005, Three-Dimensional Reservoir Characterisation and Flow Simulation of Heterolithic Tidal Sandstones, AAPG Bulletin, v. 89, n°4, p. 507-528.

Jackson, M. D., G. J. Hampson and R. P. Sech, 2009. Three-dimensional modeling of a shoreface-shelf parasequence reservoir analog: part 2. Geologic controls on fluid flow and hydrocarbon recovery : AAPG Bulletin, v. 93, p. 1183–1208.

Jackson, M. D., J. L. M. A. Gomes, P. Mostaghimi, J. R. Percival, B. S. Tollit, D. Pavlidis, C. C. Pain, A. H. El-Sheikh, A. H. Muggeridge, and M. J. Blunt, in press, Reservoir modeling for flow simulation using surfaces, adaptive unstructured meshes and an overlapping control-volume-finite-element method: Society of Petroleum Engineers Reservoir Evaluation and Engineering.

King, P. R., 1990, The connectivity and conductivity of overlapping sand bodies, in A. T. Buller, E. Berg, O. Hjelmeland, J. Kleppe, O. Torsaeter, and J. O. Aasen, eds., North Sea oil and gas reservoirs II: London, United Kingdom, Graham and Trotman, p. 353–361.

Kjønsvik, D., J. Doyle, T. Jacobsen, and A. Jones, 1994, The effects of sedimentary heterogeneities on production from a shallow marine reservoir – What really matters?, SPE Annual Technical Conference and Exhibition, New Orleans, USA, 25-28 September, Society of Petroleum Engineers paper 28445.

Legler, B., H. D. Johnson, G. J. Hampson, B. Y. G. Massart, C. A.-L. Jackson, M. D. Jackson, A. El-Barkooky, and R. Ravnås, 2013, Facies model of a fine-grained, tide-dominated delta: Lower Dir Abu Lifa Member (Eocene), Western Desert, Egypt, Sedimentology, v. 60, p. 1313-1356.

Martinius, A. W., P. S. Ringrose, C. Brostrøm, C. Elfenbein, A. Næss, and J. E. Ringås, 2005, Reservoir Challenges of Heterolithic Tidal Sandstone Reservoirs in Halten Terrace, mid-Norway, Petroleum Geoscience, v. 11, n°1, p. 3-16.

Martinius, A. W., and J. H. van den Berg, 2011, Atlas of sedimentary structures in estuarine and tidally-influenced river deposits of the Rhine-Meuse-Scheldt system, EAGE Publications BV, Houten, 298 pp.

Massart, B. Y. G., M. D. Jackson, G. J. Hampson, H. D. Johnson, B. Legler, and C. A-L. Jackson, 2016, Effective flow properties of heterolithic, cross-bedded tidal sandstones: Part 1. Surface-based modeling, AAPG Bulletin, this issue.

Nio, S.-D., and C.-S. Yang, 1991, Diagnostic Attributes of Clastic Tidal Deposits: a Review, Clastic Tidal Sedimentology, Canadian Society of Petroleum Geologists, Memoir 16, p. 3-28.

Nordhal, K., P. S. Ringrose, and R. Wen, 2005, Petrophysical Characterisation of a Heterolithic Tidal Reservoir Interval Using a Process Based Modelling Tool, Petroleum Geoscience, EAGE/Geological Society of London, v. 11, p. 17-28.

Nordahl, K., and P. S. Ringrose, 2008, Identifying the Representative Elementary Volume for Permeability in Heterolithic Deposits Using Numerical Rock Models, Math Geoscience, v. 40, p. 753-771.

Pickup, G. E., P. S. Ringrose, M. M. Forrester, J. L. Jensen, K. S. Sorbie, A. Rezigh, 1994, The Geopseudo Atlas; geologically based upscaling of multiphase flow, Society of Petroleum Engineers paper 27565.

Pickup, G. E., and D. Carruthers, 1996, Effective flow parameters for 3D reservoir simulation, Society of Petroleum Engineers paper 35495.

Pickup, G. E., and K. S. Sorbie, 1996, The scaleup of two-phase flow in porous media using phase permeability tensors, Society of Petroleum Engineers paper 28586.

Pickup, G. E., P. S. Ringrose, A. Sharif, 2000, Steady-state upscaling; from lamina-scale to full-field model, Society of Petroleum Engineers Journal, v. 5, p. 208-217.

Reineck, H. E., and I. B. Singh, 1980, Depositional sedimentary environments with reference to terrigenous clastics, 2nd edition, Springer-Verlag, Berlin.

Ringrose, P. S., K. S. Sorbie, P. W. M. Corbett, and J. L. Jensen, 1993, Immiscible flow behaviour in laminated and cross-bedded sandstones, Journal of Petroleum Science and Engineering, v. 9, p. 103-124.

Ringrose, P. S., E. Skjetne, and C. Elfenbein, 2003, Permeability Estimation Functions Based on Forward Modelling of Sedimentary Heterogeneity, Society of Petroleum Engineers paper 84275, presented at the SPE Annual Technical Conference and Exhibition held in Denver, Colorado, USA, 5–8 October.

Ringrose, P. S., K. Nordhal, and R. Wen, 2005, Vertical Permeability Estimation of Heterolithic Tidal Deltaic Sandstones, Petroleum Geoscience, EAGE/Geological Society of London, v. 11, n°1, p. 29-36.

Rubin, D. M., 1987), Cross-bedding, bedforms, and palaeocurrents. Concepts in Sedimentology and Paleontology, Society of Economic Palaeontologists and Mineralogists Special Publication, v. 1.

Sech, R. P., M. D. Jackson, and G. J. Hampson, 2009, Three-Dimensional Modelling of a Shoreface-Shelf Parasequence Reservoir Analog: Part 1. Surface-based Modelling to Capture High Resolution Facies Architecture, AAPG Bulletin, v. 93, n°9, p. 1155-1181.

Terwindt, J. H. J., 1971, Lithofacies of inshore estuarine and tidal inlet deposits, Geologie en Mijnbouw, v. 50, p. 515-526.

Warren, J. E., and H. S. Price, 1961, Flow in heterogeneous porous media, Society of Petroleum Engineers Journal, v. 1, p. 153-169.

Weber, K. J., 1982, Influence of Common Sedimentary Structures on Fluid Flow in Reservoir Models, Society of Petroleum Engineers Paper 9247.

Weber, K. J., 1986, How heterogeneity affects oil recovery *in* Lake, L. W., and H. B. Carroll Jr. (eds), Reservoir characterisation, Academic Press (New York), p. 487-544.

Wen, R.-J., A. W. Martinius, A. Næss, and P. S. Ringrose, 1998, Three dimensional simulation of small-scale heterogeneity in tidal deposits – A process-based stochastic method *in* Buccianti, A., G. Nardi, and A. Potenza (eds), Proceedings of the 4th Annual Conference of the International Association of Mathematical Geology, Ischia, De Frede, Naples, p. 129–134.

White, C. D., and M. D. Barton, 1999, Translating outcrop data to flow models, with applications to the Ferron Sandstone: Society of Petroleum Engineers Reservoir Evaluation and Engineering, v. 2, p. 341–350.

White, C. D., B. J. Willis, S. P. Dutton, J. P. Bhattacharya, and K. Narayanan, 2004, Sedimentology, statistics, and flow behavior for a tide-influenced deltaic sandstone, Frontier Formation, Wyoming, United States, in G. M. Grammer, P. M. Harris, and G. P. Eberli, eds., Integration of outcrop and modern analogs in reservoir modeling: AAPG Memoir 80, p. 129–152.

749 White, C. D., B. J. Willis, K. Narayanan, and S. P. Dutton. 2001. Identifying and Estimating
750 Significant Geological Parameters with Experimental Design: SPE Reservoir Evaluation and
751 Engineering v. 6, p.311-324.

752

753 **AUTHOR VITAE**

754 Benoît Y. G. Massart works in the mature-area developments and increased oil recovery
755 team at the Statoil research center in Bergen, Norway. He holds a Ph.D. in petroleum
756 engineering from Imperial College London and a M.Sc. in petroleum geology from the École
757 Nationale de Géologie de Nancy (ENSG), France. His research interests are in reservoir
758 modeling and quantifying the influence of geologic heterogeneity on effective rock
759 properties and fluid flow behavior.

760

761 Matthew D. Jackson is the Total professor of geological fluid mechanics in the Department of
762 Earth Science and Engineering, Imperial College London. He holds a B.S. degree in physics
763 from Imperial College and a Ph.D. in geological fluid mechanics from the University of
764 Liverpool. His research interests include simulation of multiphase flow through porous
765 media, representation of geologic heterogeneity in simulation models, and downhole
766 monitoring and control in instrumented wells.

767 Gary J. Hampson is a Reader in sedimentary geology in the Department of Earth Science and
768 Engineering, Imperial College London. He holds a B.A. degree in natural sciences from the
769 University of Cambridge and a Ph.D. in sedimentology and sequence stratigraphy from the
770 University of Liverpool. His research interests lie in the understanding of depositional
771 systems and their preserved stratigraphy, and in applying this knowledge to reservoir
772 characterization.

773

774 Howard D. Johnson holds the Shell Chair of Petroleum Geology in the Department of Earth
775 Science and Engineering, Imperial College London. His main interests are in clastic
776 sedimentology, sequence stratigraphy, reservoir characterization, and basin studies.
777 Previously, he spent 15 years with Shell working in research, exploration and development
778 geology, and petroleum engineering. He holds a B.Sc. degree in geology from the University
779 of Liverpool and a D.Phil. in sedimentology from the University of Oxford.

780

781 ## Figure captions

782

783 **Figure 1:** Plot illustrating the variation in a measured reservoir property for different sample
784 volumes (Bear, 1972). Small sample volumes exhibit a wide range of values for the measured
785 property, indicating that these volumes are unrepresentative of reservoir behavior. A
786 representative value of the measured property is obtained for larger sample volumes, above
787 a threshold defined by the representative element volume (REV).

788

789

790 **Figure 2:** Intermediate surface-based model of trough cross-bedded tidal sandstone,
791 generated using input parameters extracted from the Gecko Nose outcrop analog (see
792 Figure 3 in Massart *et al.*, 2016). The model presented here contains foreset-toeset surfaces
793 that are entirely covered with mudstone drapes in black (i.e. 100% mudstone coverage). Dip,

794 strike and vertical orientations are defined related to the orientation of the cross-bedding
795 surfaces. The conditions of a flow simulation experiment in the dip orientation are
796 represented on the figure: the inlet and outlet injection and production faces are
797 reproduced with colored rectangles, corresponding to the buffer zones of high permeability
798 introduced to ensure homogeneous flow injection and production.

799

800 **Figure 3:** A) Outcrop photograph of one cross-bed set featuring trough cross-bedding lined
801 with mudstone drapes. The red dotted line Γ corresponds to the boundary between foreset
802 and toeset parts of the cross-bed set. B) View of the trough cross-bedded end-member
803 model of cross-bedded sandstones used to investigate the sensitivity of effective
804 permeability to geometric input parameters (Table 1). Cross-bedding surfaces are colored
805 depending on the depth value in each cross-bed set. The rectangle indicates the position of
806 the cross-sections C and D. C) Dip-oriented cross-section illustrating foreset-toeset surfaces
807 in the model, with the boundary between foreset and toeset parts identified in each cross-
808 bed set, and D) dip-oriented cross-section showing 25% mudstone drape coverage along
809 foresets in the model.

810

811 **Figure 4:** A) Outcrop photograph of tabular cross-bed sets with foreset-toeset surfaces lined
812 with mudstone drapes. B) View of the tabular cross-bedded end-member model of cross-
813 bedded sandstones used to investigate the sensitivity of effective permeability to geometric
814 input parameters (Table 1). Cross-bedding surfaces are colored following their depth value in
815 each cross-bed set. The rectangle indicates the position of the cross-sections C and D. C) Dip-

oriented cross-section illustrating foreset-toeset surfaces in the model, and D) dip-oriented cross-section showing 25% mudstone drape coverage along foresets in the model.

Figure 5: Control of the water pressure during single-phase flow simulation of the surface-based intermediate model with 25% mudstone drape coverage. The injection and production wells are controlled by bottom hole pressure, so flow rates vary through time. The horizontal axis represents the amount of pore volumes injected in the model, calculated by dividing the volume of water injected by the entire pore volume of the model. Effective permeability of the model is calculated at steady state, when both injection and production flow rates become constant and equal, and when the average field pressure remains constant. Steady-state is achieved in a very short period (4×10^{-7} of the entire pore volume of the model is injected in 18 s), due to the incompressibility of the fluids and the very small compressibility of the rocks.

Figure 6: Normalized effective horizontal permeability versus sample volume. Samples are always located at the center of the intermediate model of heterolithic, cross-bedded tidal sandstones (Figure 2); mudstone drape coverage along foreset-toeset surfaces is 25%. Error bars represent the numerical artefacts introduced by the cornerpoint grid, calculated for models without mudstone (100% sandstone). The values of effective permeability are normalized by the calculated permeability of the equivalent sample containing only sandstone.

838 **Figure 7:** Normalized effective permeability for the intermediate model of heterolithic, cross-
839 bedded tidal sandstones (Figure 2), for varying sandstone content. Effective permeability is
840 measured in three orthogonal directions: k_d, k_s and k_v. The shaded areas correspond to the
841 error in calculated permeability introduced by the cornerpoint grid.

842

843 **Figure 8:** Normalized effective permeability of the intermediate, trough cross-bedded end-
844 member, and tabular cross-bedded end-member models: A) dip-oriented effective
845 horizontal permeability k_d for models with wavy-bedded toesets, B) strike-oriented effective
846 horizontal permeability k_s for models with wavy-bedded toesets, C) k_d for models with
847 lenticular-bedded toesets, and D) k_s for models with lenticular-bedded toesets. Dashed lines
848 correspond to results discussed in the text.

849

850 **Figure 9:** Dip-oriented cross-sections through the (A and B) trough cross-bedded end-
851 member (Figure 3), (C and D) intermediate (Figures 2) and (E and F) tabular cross-bedded
852 end-member (Figure 4) models, showing the fluid potential at steady-state, with 25%
853 mudstone drape coverage along foresets for each model. Toesets are modelled as wavy-
854 bedded in A), C) and E), and as lenticular-bedded in B), D) and F).

855

856 **Figure 10:** Tornado charts summarizing the impact on effective permeability of variations in
857 six geometric input parameters in the dip (A – C) and strike (D – F) directions. Three
858 scenarios of mudstone drape coverage along foreset-toeset surfaces are presented: (A, D)

have 100% coverage of foresets; (B, E) have 25% coverage of foresets; (C, F) have 0% coverage of foresets. Geometric parameters and their settings are summarized in Table 1.

861 **Table captions**

862

863 **Table 1:** Input parameters for the intermediate model used to evaluate the effect of volume
864 sampling, and for the two end-member settings used to model and to analyze the sensitivity
865 of effective permeability to six geometric parameters (shaded in grey) that control cross-
866 bedding style.

867

868 **Table 1:**

Input parameter	Symbol	Unit	Intermediate model	Trough cross-bedding end-member model	Tabular cross-bedding end-member model
Volume of the model	V_T	m^3	9	9	9
Elemental volume density	D	m^{-3}	6 elemental volumes in 9 m^3	6 elemental volumes in 9 m^3	4 elemental volumes in 9 m^3
Number of cross-bedding surfaces	N_{CB}	-	≈600	≈540	≈170
Style of cross-bedding	-	-	Trough	Trough	Tabular
Parabolic curvature of foreset-toeset template surfaces	A	-	5.5 x 10-3	5.5 x 10-3	5.5 x 10-3
Foreset thickness	F_T	cm	5.9 ± 3.9	5.9 ± 3.9	10 ± 3.9
Toeset dip angle	α	°	8	8	1
Angle of dune climb	δ	°	5	5	0
Mudstone frequency function	$f(M,N,O)$	-	Function f (Figure 12)	Function f (Figure 12)	Function f (Figure 12)
Mudstone patch length	MPL	cm	[10 – 20] Uniform distribution	[10 – 20] Uniform distribution	[10 – 100] Uniform distribution
Mudstone patch width	MPW	cm	[10 – 20] Uniform distribution Smaller than MPL	[10 – 20] Uniform distribution Smaller than MPL	[10 – 100] Uniform distribution Smaller than MPL
Minimum mudstone patch area	MPS	cm^2	150	150	150
Foreset to toeset volume ratio	$R_{F/T}$	-	6.5 : 1 (87% foresets; 13% toesets)	2 : 3 (40% foresets; 60% toesets)	24 : 1 (96% foresets; 4% toesets)

869

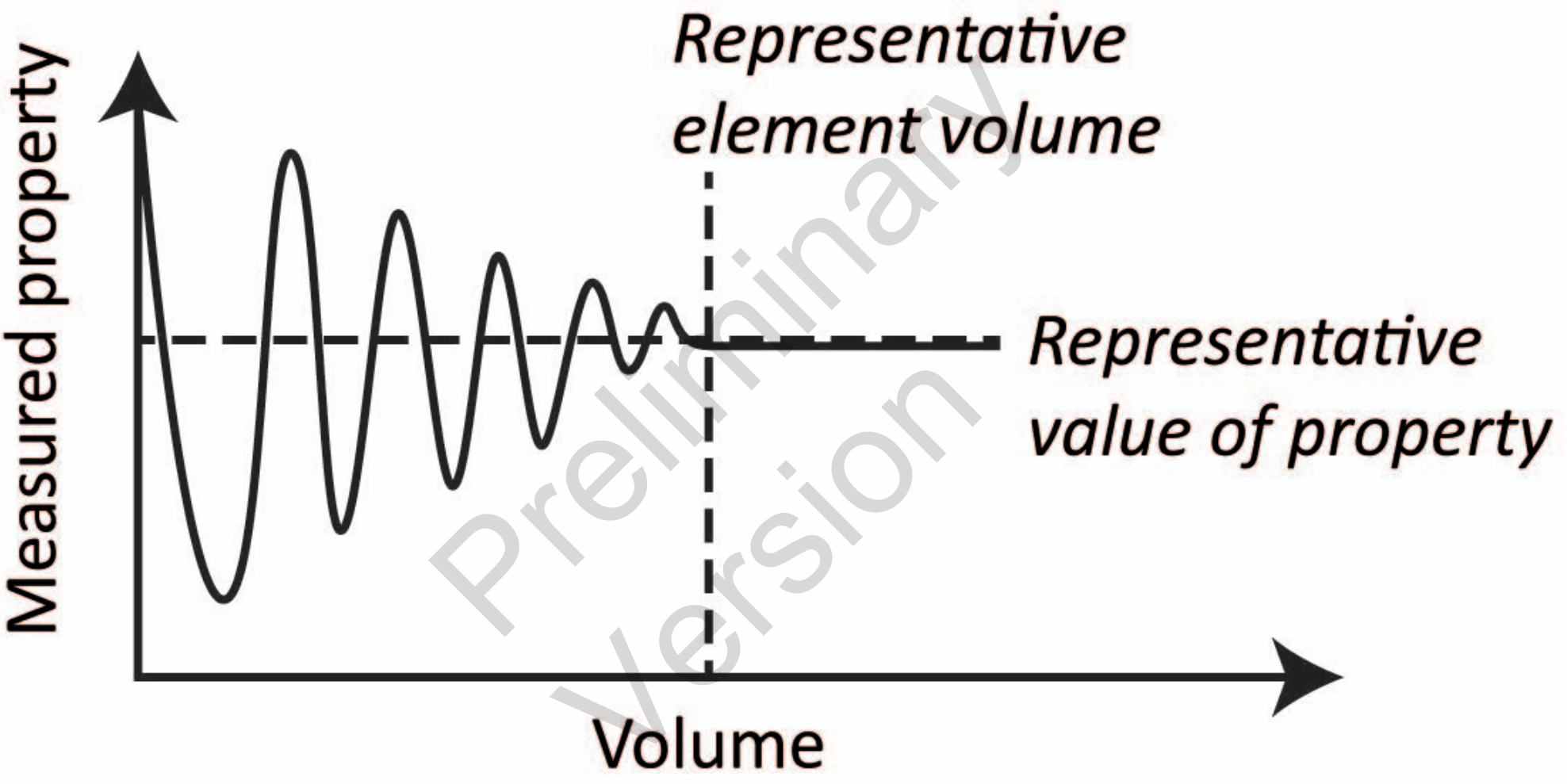

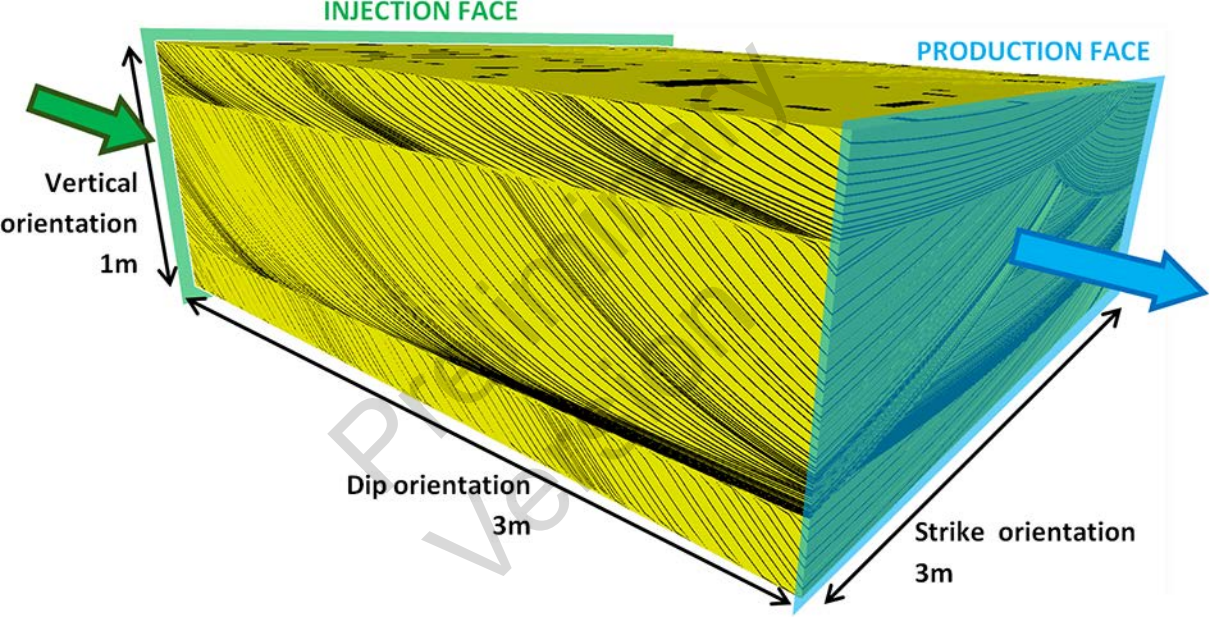
INJECTION FACE
PRODUCTION FACE
Vertical orientation 1m
Dip orientation 3m
Strike orientation 3m

A)

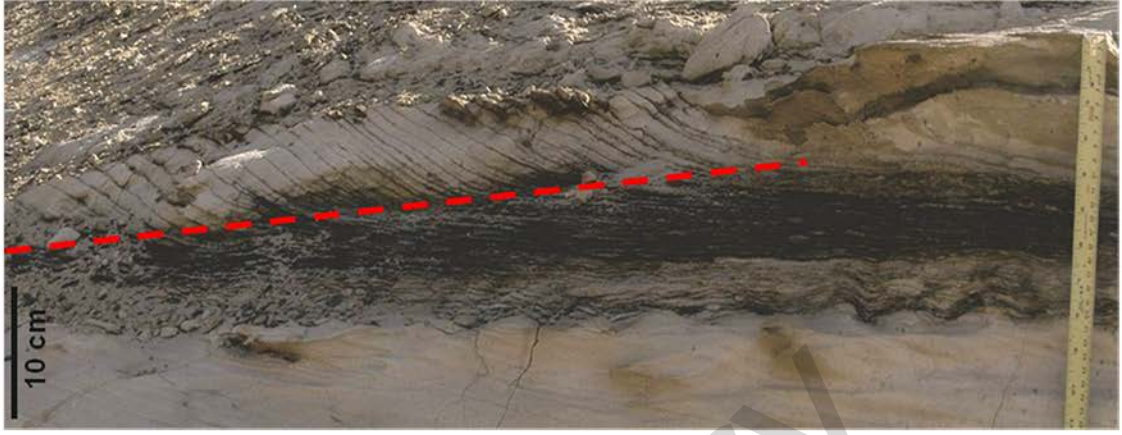

B)

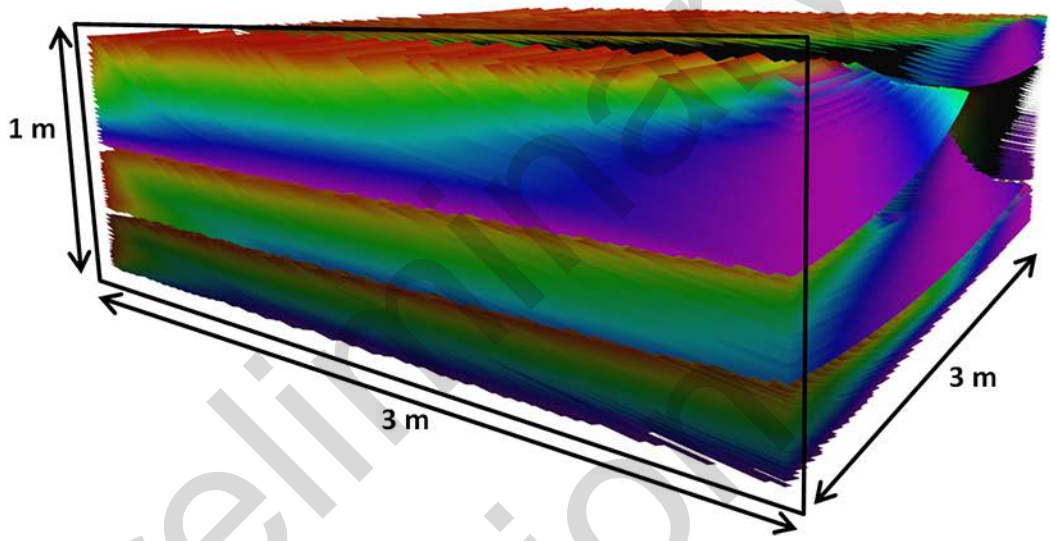

C)

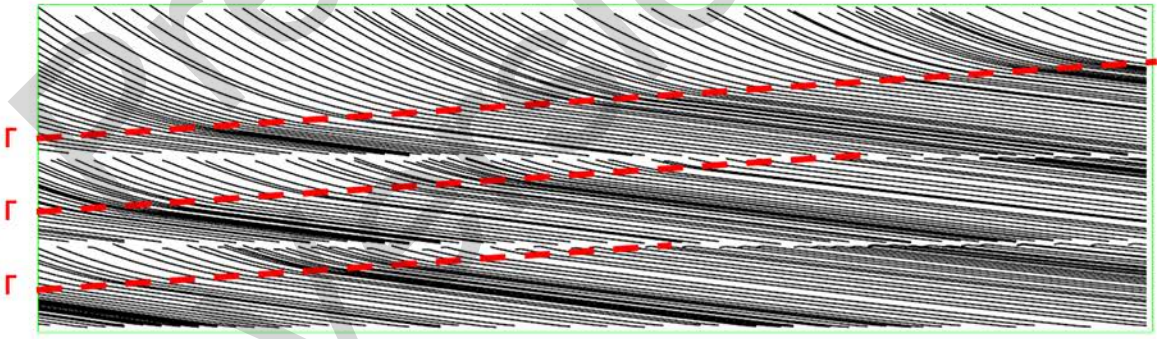

D)

A)

B)

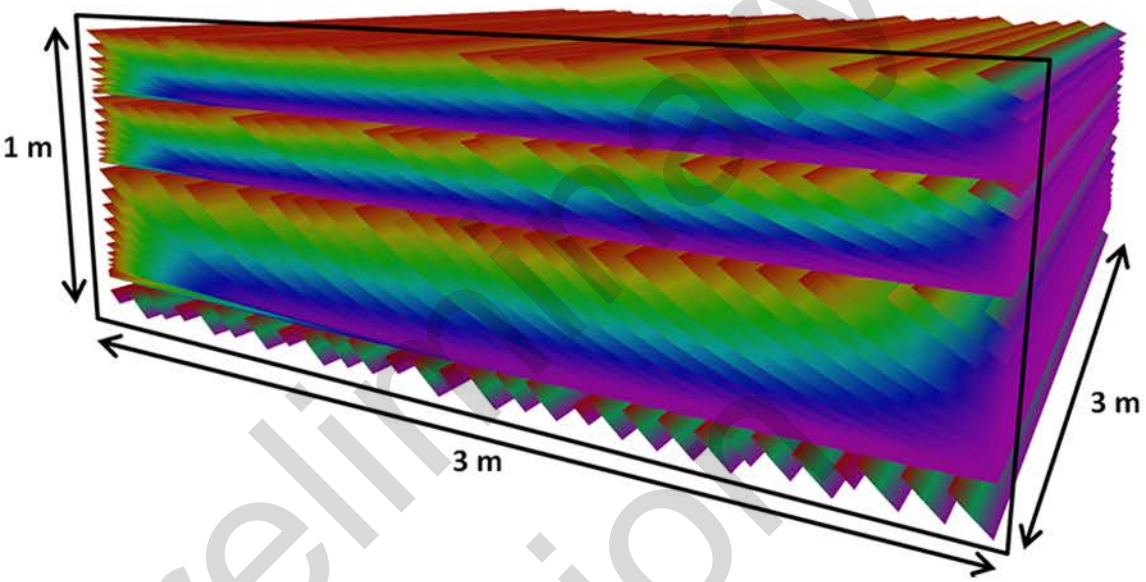

C)

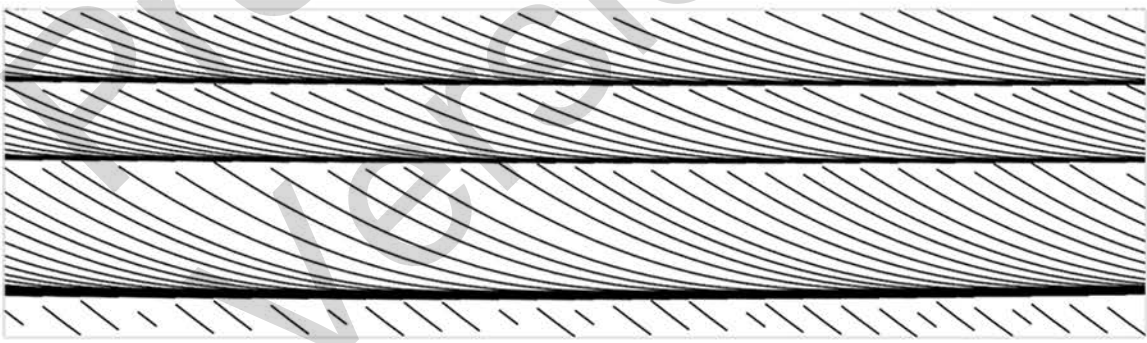

D)

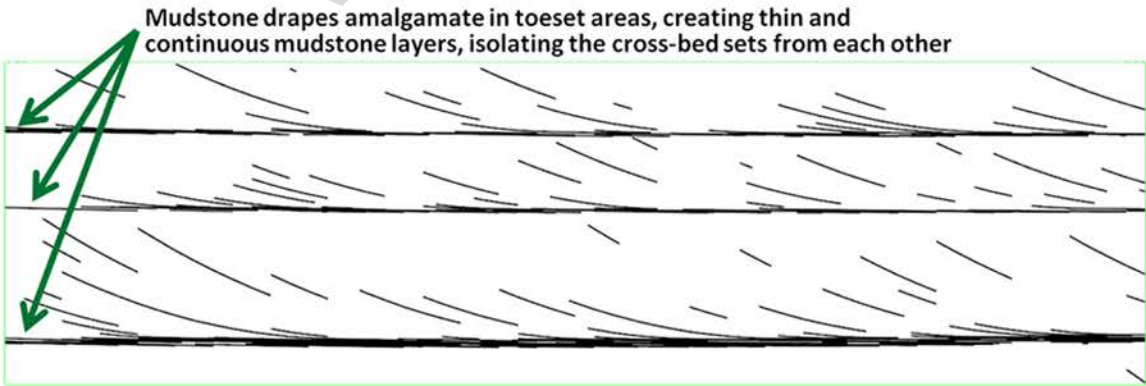

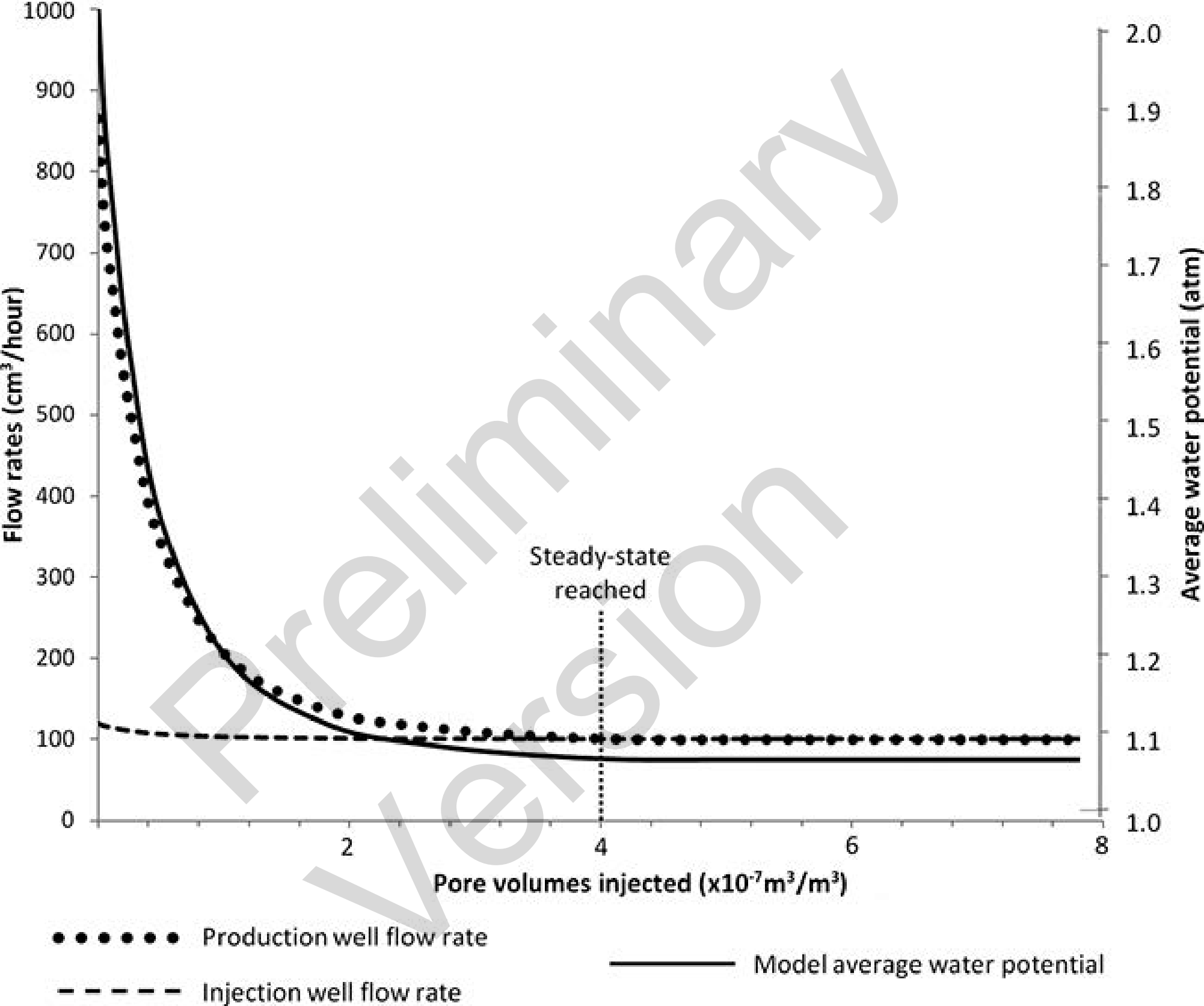

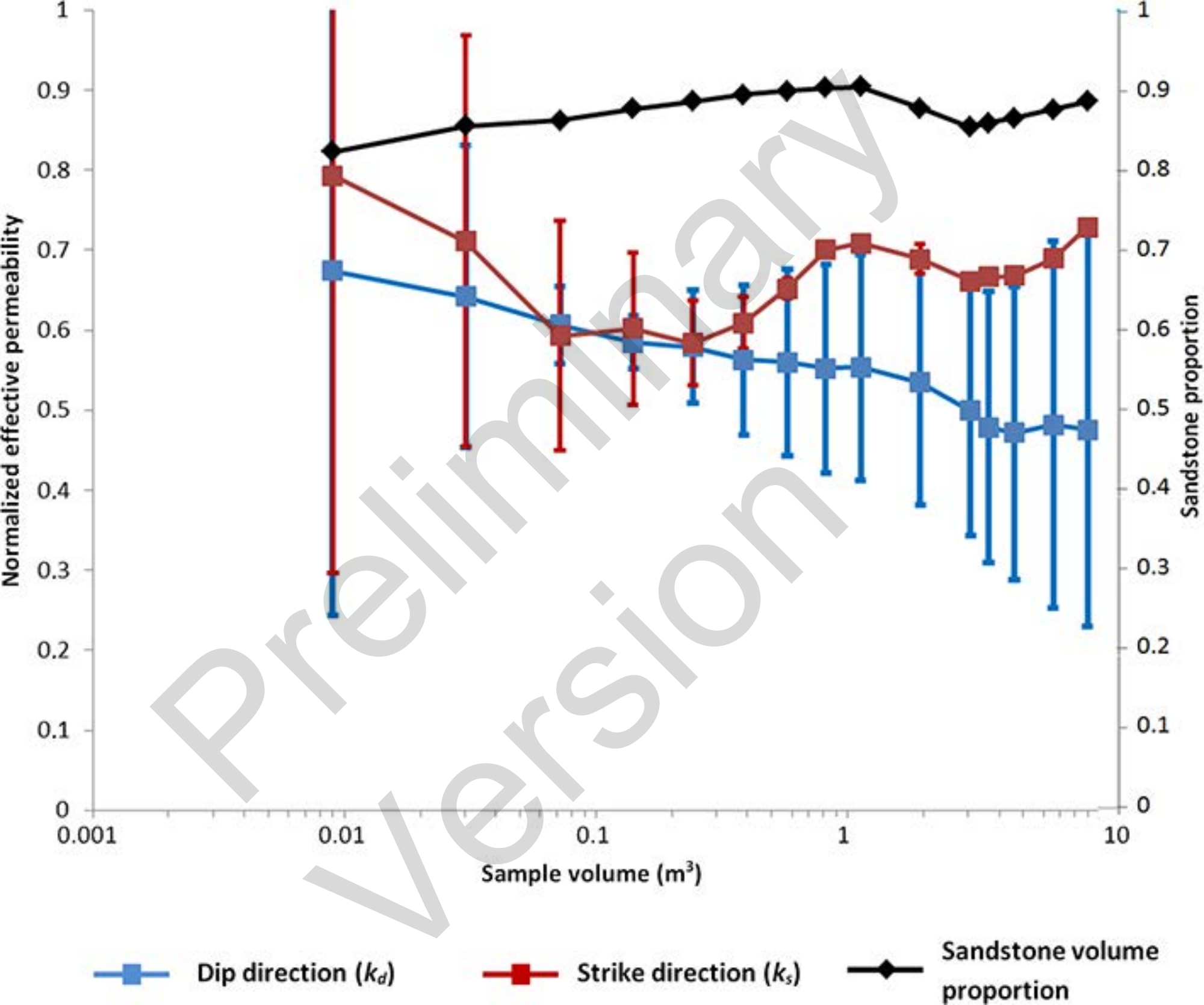

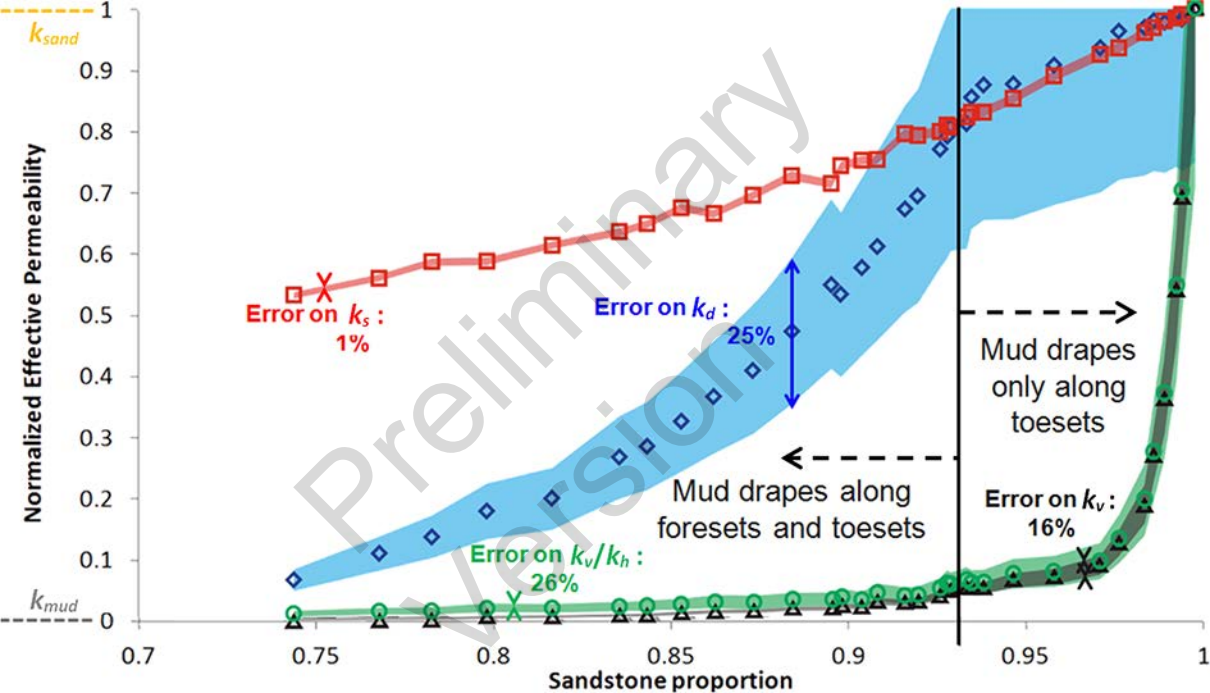
k_{sand}
k_{mud}
Normalized Effective Permeability
1
0.9
0.8
0.7
0.6
0.5
0.4
0.3
0.2
0.1
0
Error on k_s : 1%
Error on k_d : 25%
Error on k_v/k_h : 26%
Error on k_v : 16%
Mud drapes only along toesets
Mud drapes along foresets and toesets
0.7
0.75
0.8
0.85
0.9
0.95
1
Sandstone proportion
Preliminary version

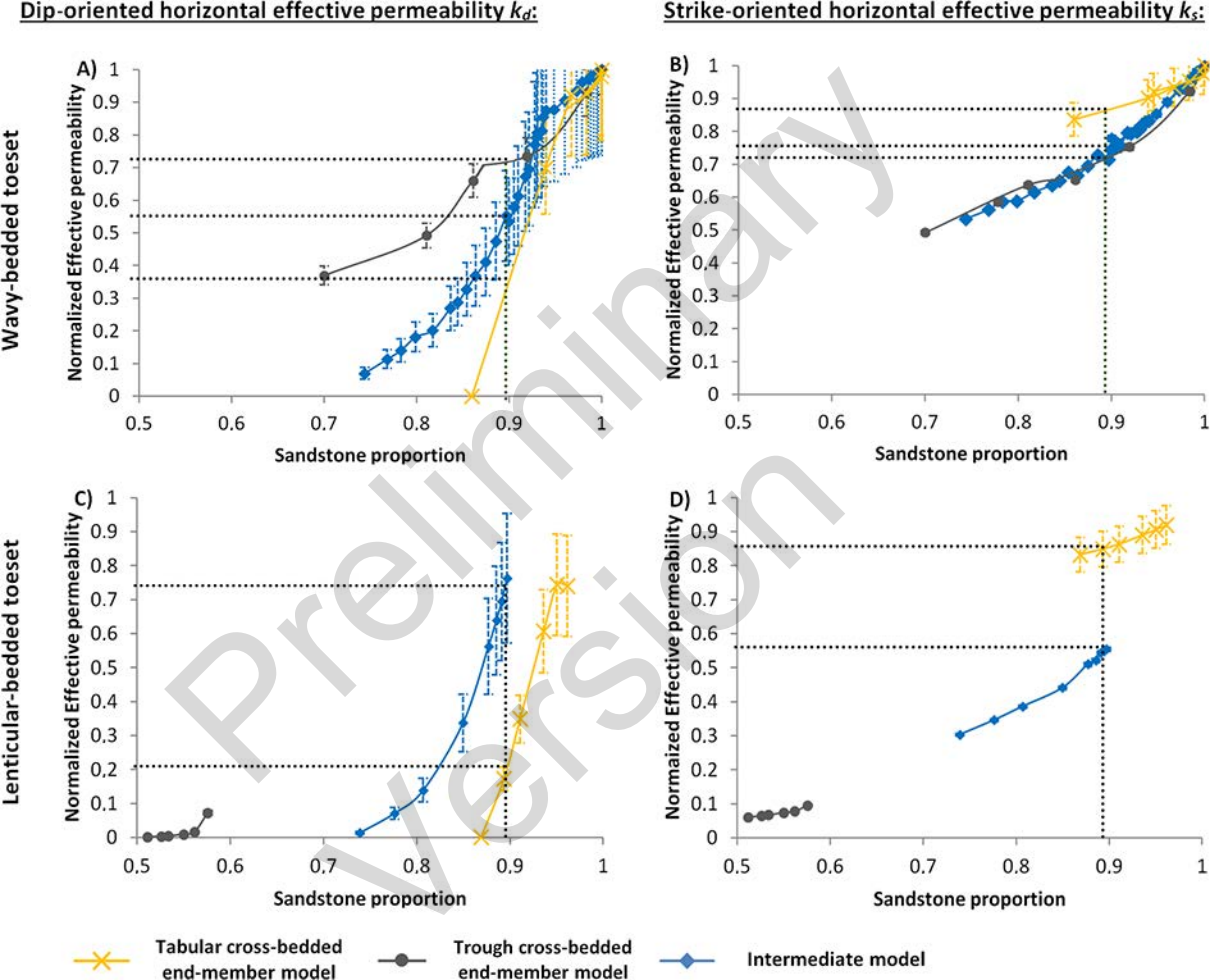
Dip-oriented horizontal effective permeability k_d:
Strike-oriented horizontal effective permeability k_s:
Wavy-bedded toeset
Lenticular-bedded toeset
A)
B)
C)
D)
Normalized Effective permeability
Sandstone proportion
Tabular cross-bedded end-member model
Trough cross-bedded end-member model
Intermediate model
Preliminary Version